



20 nitrate loading from the SWAT model, we were able to simulate nitrate concentrations in the discharged
21 groundwater as well as to simulate changes in nitrate concentrations resulting from different land use and
22 management scenarios. Critically, our approach developed here permits simulation of travel time
23 distributions and source areas of water volumes and nitrate masses. We show how these source and age
24 components can be used to guide the prioritization of water quality mitigation strategies that consider
25 both intrinsic (i.e., hydrogeological) vulnerability as well as specific management actions that could be
26 taken to improve surface water and groundwater quality.

27 **1 Introduction**

28 Groundwater contamination is a widespread global problem. Nitrate pollution in particular can lead to
29 eutrophication of water bodies and health problems in humans [Hansen et al., 2017; Zhou et al., 2015].
30 Elevated nitrate concentrations in groundwater are typically linked to the use of fertilizers in agriculture,
31 animal waste, and effluent from human wastewater disposal systems [Almasri, 2007; Craswell, 2021].
32 Alternative mitigation strategies to decrease the nitrate loading to groundwater have different costs,
33 benefits, and implementation-response timelines. Assessing the downstream response to a change in
34 nitrate loading is complex, as the fate and transport of nitrate in the subsurface is determined by coupled
35 biological, chemical, and hydrogeological processes that vary widely in time and space [Correa-González
36 et al., 2023; Lake et al., 2003; Wriedt and Rode, 2006].

37 The recently developed SWAT-MODFLOW-RT3D (SMR) code [Wei et al., 2019], is a numerical
38 simulation tool that accounts for most processes relevant to groundwater nitrate transport. In essence,
39 SWAT simulates flow and solute transport near the surface (including recharge to groundwater),



40 MODFLOW simulates groundwater flow, and RT3D simulates solute transport in the groundwater
41 domain by means of solving the advection-dispersion-reaction equation. Compared to using only
42 MODFLOW and RT3D, the key advantage of SMR is that the nitrate loading to the groundwater domain
43 does not need to be specified as a boundary condition. Instead, this loading is implicitly simulated as a
44 function of weather, soil and hydrologic conditions, land use and management systems. Thus, SMR
45 permits assessment of nitrate fate and transport under scenarios of changes in land use (including changes
46 in agricultural practices) and climate [Wei et al., 2019]. However, SMR only simulates spatiotemporal
47 variations in nitrate concentrations and does not provide direct information about source areas or travel
48 times of groundwater and nitrate. This means that while it can be used to simulate the outcome of
49 alternative strategies, it provides little information to guide optimal water quality improvement strategies
50 and does not provide immediate insights into why the outcomes of alternative mitigation strategies may
51 differ. Furthermore, as a fully coupled transport model, SMR is computationally expensive, especially for
52 large regions or highly resolved model domains.

53 In contrast, particle-tracking is widely regarded as a useful and relatively computationally efficient tool
54 for solute transport that can simulate the source and age components of groundwater as well [Engdahl et
55 al., 2016; V Kaandorp et al., 2018; Maxwell et al., 2019; Wilusz et al., 2020]. Backward particle-tracking
56 provides insight into the intrinsic vulnerability of specific regions to groundwater pollution [Medici et al.,
57 2021; Molson and Frind, 2012]. Namely, using the final location of the back-tracked particles, it is
58 possible to map pollutant source areas and associated travel times. Source areas with higher contributions
59 to the discharge volumes and shorter travel times are typically classified as more vulnerable. However,



60 applying particle-tracking to simulate nitrate transport typically requires setting an explicit boundary
61 condition for nitrate mass loading [V P Kaandorp et al., 2021; Kauffman, 2001; Mullaney, 2007].
62 Given the complexity of nitrate transport in groundwater and the limitations of current modeling
63 approaches, there is a need for more efficient and flexible methods that not only simulate nitrate
64 concentrations but also provide insights into groundwater source areas, travel times, and vulnerability to
65 pollution. In this study, we propose a novel modeling framework based on SWAT-MODFLOW [Bailey
66 et al., 2016] and MODPATH [Pollock, 2016], a particle-tracking code specifically designed for
67 MODFLOW models. Using this approach, we simulate the age and source components of discharged
68 groundwater. SWAT-MODFLOW is the same model code as SWAT-MODFLOW-RT3D except that the
69 RT3D computations are omitted. Thus, SWAT-MODFLOW simulates the nitrate loading to the aquifer
70 but does not simulate subsequent transport in the MODFLOW domain. By combining particle-tracking
71 results with the simulated nitrate loading we can simulate nitrate concentrations in discharged
72 groundwater. The age and source components of the discharged groundwater provide information about
73 the intrinsic vulnerability of the groundwater domain, which together with nitrate loadings, can be used
74 to consider alternative mitigation strategies and estimate how long they will take to affect nitrate
75 concentrations in discharge areas. Our novel approach thus overcomes some of the limitations of SMR
76 while keeping the useful feature of simulating the nitrate loading as a function of land use and weather
77 conditions, rather than specifying it as a boundary condition.

78 We apply this modeling framework to the Santa Fe River Basin in north-central Florida, which is fed in
79 large part by discharge from springs, many of which have been identified as impaired because of high
80 nitrate levels [FDEP, 2018]. According to the Florida Springs and Aquifer Protection Act, the Florida



81 Department of Environmental Protection (FDEP) is required to delineate a priority focus area (PFA) for
82 each impaired spring system by considering groundwater travel times, hydrogeology, and nutrient loads
83 [FDEP, 2018]. A basin management action plan (BMAP) is then designated for the PFA to reduce
84 pollutant loading, which can be accomplished by adoption of best management practices, improvement
85 in wastewater treatment and disposal, conservation programs, and other water quality improvement
86 projects. Given this context, this study aims to: (1) develop a novel modeling framework that combines
87 SWAT-MODFLOW and MODPATH to simulate groundwater flow and nitrate transport in terms of age
88 and source components; (2) apply and test this framework in the Santa Fe River Basin to quantify the
89 contributions of different land uses to nitrate pollution and assess groundwater travel times; and (3)
90 provide actionable insights into the prioritization of nitrate mitigation strategies based on the travel time
91 and source area contributions to groundwater nitrate pollution.

92

93 **2 Modeling Framework**

94 **2.1 Overview of Modeling Framework**

95 Our overall model integration framework and workflow is summarized in Figure 1, and each step is
96 described in detail below. Briefly, the first step is to build, calibrate, and validate one or more SWAT-
97 MODFLOW models of the target domain. Next, a stand-alone MODFLOW model, adapted from the
98 SWAT-MODFLOW model(s) in step 1, is developed on a coarser temporal timescale and used along with
99 MODPATH to simulate particle-tracking in the final step. While the modeling framework uses three



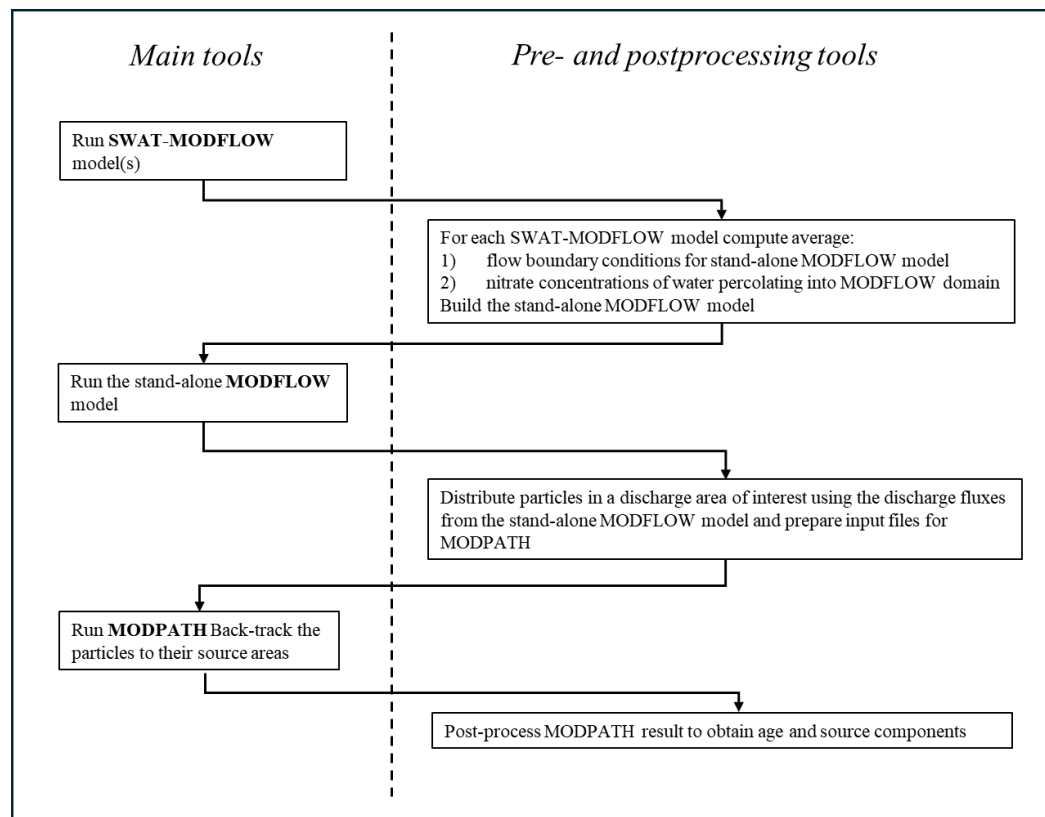
100 existing simulation codes (SWAT-MODFLOW, MODFLOW, and MODPATH), some additional codes
101 for pre- and post-processing are also required (Figure 1).

102

103 **2.2 SWAT-MODFLOW Model(s)**

104 The Soil Water Assessment Tool (SWAT) (Arnold et al., 1998) is a widely used watershed model. In
105 SWAT, the watershed is divided into hydrologic response units (HRUs), which are areas within a subbasin
106 that share the same slope, soil, and land use characteristics. In SWAT-MODFLOW (Bailey et al., 2016),
107 SWAT is coupled with the well-established groundwater modeling code MODFLOW-NWT (Niswonger
108 et al., 2011; Harbaugh, 2005) from the United States Geological Survey (USGS). The process of creating
109 the linkage files needed to build a SWAT-MODFLOW model is described in existing literature (Bailey
110 et al., 2016; Park and Bailey, 2017; Park et al., 2019). These linkage files define how to partition fluxes
111 from HRU's to MODFLOW grid cells. As explained in more detail below, it can be useful to build more
112 than one SWAT-MODFLOW model, each based on a static land use map, to analyze changes in nitrate
113 loading due to changes in land use.

114



115

116 **Figure 1.** Schematic illustrating the modeling framework.

117

118 **2.3 Stand-Alone MODFLOW Model**

119 MODPATH is a particle-tracking code for MODFLOW that is based on computationally efficient semi-
120 analytical solutions that track each particle through a single cell in a single step as long as the flow field
121 remains constant during this tracking step (Pollock, 2016). However, for flow fields that vary on a daily
122 basis, as is the case in SWAT-MODFLOW, this process can be computationally inefficient, particularly
123 since the time period covered by the flow fields must be long enough to simulate complete particle
124 trajectories. Our modeling framework circumvents these issues by using a separate, stand-alone



125 MODFLOW model. From the SWAT-MODFLOW output, we compute the average flow boundary
126 conditions for effective groundwater recharge and well pumping over longer time periods, reducing the
127 number of changes in the flow field and enhancing computational efficiency by limiting the number of
128 semi-analytical tracking steps. As explained further in Appendix A, due to an error in the original SWAT-
129 MODFLOW code, we modified the code to transfer water between MODFLOW groundwater cells and
130 SWAT river reaches using differences between groundwater elevation and the river bottom. As a result,
131 transient river stages in SWAT do not affect the MODFLOW simulations, obviating the need to average
132 their stages for the stand-alone MODFLOW model. We note that our approach assumes boundary
133 conditions can be averaged over longer periods without significantly affecting particle-tracking results;
134 this assumption is reasonable if boundary conditions fluctuate around a mean on timescales much smaller
135 than groundwater travel times.

136 The stand-alone MODFLOW model allows us to easily simulate transitions between alternative land use
137 and land management scenarios. Namely, we can define multiple stress periods to account for different
138 boundary conditions as computed from specific SWAT-MODFLOW models with different land use and
139 land management configurations. Depending on groundwater travel time distributions, it may be
140 necessary to account for historic land uses when simulating groundwater nitrate concentrations emerging
141 in river reaches at a particular point in time. That is, some particles may need to be tracked though a time
142 period when the land use was different from what it is during the time when the particles emerge in the
143 river. Therefore, in this study we define an initial steady-state stress period using the averaged boundary
144 conditions computed from a SWAT-MODFLOW model that represents pre-development land use
145 conditions. Changes from pre-development conditions are then defined in subsequent stress periods, each



146 requiring one or more separate SWAT-MODFLOW models to compute average boundary conditions. As
147 discussed later in section 3.3, it is possible to combine multiple SWAT-MODFLOW models to compute
148 the average boundary conditions for a stress period.

149 In this study, we use steady state stress periods in the stand-alone MODFLOW model. Switching between
150 steady-state flow models to reflect changes in land use assumes that the change in the flow boundaries
151 has a relatively immediate effect on the flow field compared to groundwater travel times. However, if
152 needed, the methodology can incorporate transient stress periods to account for a more gradual change in
153 the flow field. It is also noted that if changes in land use occur gradually over a relatively long time, an
154 interpolation procedure could be used to define a gradual change in boundary conditions.

155 **2.4 Particle-Tracking**

156 In this study, we exclusively use backward tracking of particles. This is the most efficient method for
157 computing the travel time distributions and nitrate concentration within the discharge area of interest at a
158 particular point in time since all the tracked particles will contribute to these computations. Using the
159 head file created by the stand-alone MODFLOW model, we reconstruct the groundwater discharges to
160 stream reaches in our area of interest, which occur at either river or drain cells. We distribute particles
161 across these discharge cells in proportion to their flow rate such that each particle corresponds to the same
162 volumetric discharge, ensuring that each particle contributes equally to the travel time distribution. Within
163 each discharge cell we distribute the particles across the discharge area using a uniform random number
164 generator.



165 Travel time distributions of the discharged water volumes are then directly computed from the standard
166 output from MODPATH by counting the number of particles with a travel time less than τ , and dividing
167 by the total number of particles:

168

169
$$g_v(\tau, t) = \frac{1}{n} \sum_{i=1}^n \mathbf{1}_{\tau_i(t) \leq \tau} \quad (1)$$

170 where $g_v(\tau, t)$ is the cumulative distribution function for particles at time t , n is the number of particles,
171 τ_i is the travel time of particle i and $\mathbf{1}$ the indicator function (which has a value of 1 when the condition
172 $\tau_i(t) \leq \tau$ is met and 0 otherwise).

173

174 2.5 Linking Particles to Nitrate Loading

175 The concentration, c , of the discharged water is a function of the travel time distribution and is given by
176 the following response function (Benettin et al., 2022; Rodriguez et al., 2021):

177

178
$$c(t) = \int_0^\infty \iint_A c_{in}(x, y, t - \tau) e^{-k\tau} p_v(\tau, t) dx dy d\tau \quad (2)$$

179 where c_{in} is the nitrate concentration of groundwater discharged in the region of interest at time t , τ is the
180 travel time, k is the denitrification rate, A the source area and $p_v(\tau, t)$ is the fraction of water parcels with



181 travel times equal to τ , as derived from the travel time probability density function. It is noted that equation
182 2 implies that denitrification is a first-order rate process.

183 Using the particle-tracking results, the concentration of each discharged particle at time t is computed
184 from the following numerically equivalent equation:

185

186
$$c_{\text{out},i}(t) = c_{\text{in},i}(t - \tau_i) e^{-k\tau_i} \quad (3)$$

187 where $c_{\text{in},i}(t - \tau_i)$ is the nitrate concentration associated with the endpoint of particle i at time $t - \tau_i$. The
188 concentration of discharged groundwater at time t is computed from:

189

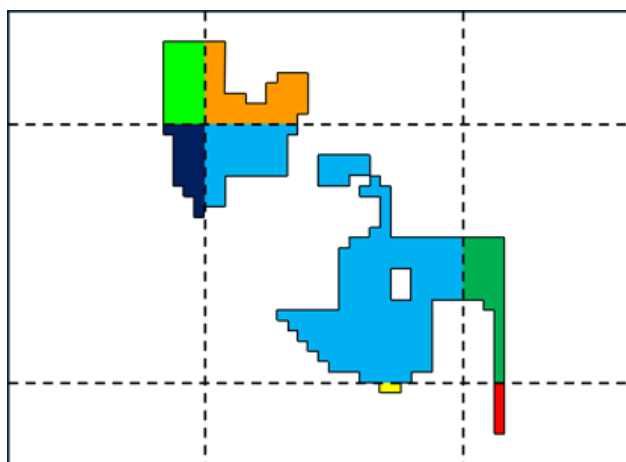
190
$$c(t) = \frac{1}{n} \sum_{i=1}^n c_{\text{out},i}(t) \quad (4)$$

191 To compute $c_{\text{in},i}$ it is important to consider the relationship between SWAT HRUs and MODFLOW raster
192 cells. As shown in Figure 2, HRUs overlap with MODFLOW cells and can be subdivided into different
193 “overlap areas”. These overlap areas are defined in linkage files and dictate how the fluxes from SWAT
194 HRUs are distributed among MODFLOW cells. The nitrate concentrations $c_{\text{in},i}$ at the surface of the
195 MODFLOW domain are computed on these overlap areas using values for the nitrate mass loading and
196 the effective groundwater recharge flux (defined as percolation flux minus groundwater evaporation flux)
197 into the MODFLOW domain. The effective groundwater recharge flux is first computed per MODFLOW
198 raster cell using HRU values for the percolation values and MODFLOW values for the groundwater
199 evaporation fluxes. Subsequently, for each overlap area the HRU percolation value is scaled such that the
200 total percolation for each MODFLOW cell equals the effective groundwater recharge flux. The nitrate



201 mass flux from each HRU is then distributed across the associated overlap areas according to the scaled
202 percolation water fluxes. Finally, the nitrate concentrations in the overlap areas are computed from the
203 nitrate mass loadings and effective groundwater recharge fluxes. Using this procedure, the nitrate
204 concentrations at the surface of the MODFLOW domain are constructed for each stress period.
205 Using the endpoint of each particle i as provided by MODPATH, it is straightforward to locate the
206 MODFLOW cell from which the particle exited the domain. To assign the particle to a particular overlap
207 area, and thus a particular HRU and land use, a transfer probability function is computed for each overlap
208 area such that the probability equals the ratio of the effective groundwater recharge flux for that overlap
209 area to the effective groundwater recharge flux for the entire MODFLOW cell. Thus, this probability
210 function accounts for a non-uniform distribution of overlap area fluxes. A random number generator is
211 used to allocate the particle to a particular overlap area with the MODFLOW cell from which the particle
212 originated and its associated concentration $c_{in,i}$. Transfer probability functions for particles for distributing
213 particles based on volumetric fluxes have previously been used in surface-subsurface flow models and
214 matrix-fracture flow models (De Rooij et al., 2012; Visser et al., 2009; Pan and Bodvarsson, 2002).

215



216



217 **Figure 2.** A single HRU subdivided into overlap areas (each color represents a separate overlap area) by
218 its intersection with the MODFLOW raster (black dashed lines).

219

220 Since we can link each particle with a nitrate concentration in the source area, and each particle is assumed
221 to represent the same volumetric flux, it is then relatively straightforward to compute the travel time
222 distributions of discharged nitrate masses:

223

$$g_m(\tau, t) = \frac{1}{\sum_{j=1}^n c_{out,j}(t)} \sum_{i=1}^n c_{out,i}(t) \mathbf{1}_{\tau_i \leq \tau} \quad (5)$$

224 where $g_m(\tau, t)$ is the cumulative travel time distribution of nitrate mass for particles. Note that once
225 particles are associated with HRUs, we can also associate a land use with each particle and thus construct
226 travel time distributions for each land use component.

227 2.6 Intrinsic Vulnerability Mapping

228 Backward particle-tracking results are useful to gain insight into the intrinsic vulnerability of watersheds
229 (Molson and Frind, 2012; Medici et al., 2021). Using the final location of the back-tracked particles, it is
230 possible to map source areas as well as the travel times. Source areas with higher contributions to the
231 groundwater discharge volumes and shorter travel times may be classified as more vulnerable. In this
232 study, the source area contributions and the travel times were mapped to a raster with the same resolution
233 as used for the HRU mapping in SWAT. Source area contributions were mapped as a fraction of the total
234 number of particles released and thus sum to unity. Using the simulated nitrate loadings for each HRU,
235 we also create raster maps that indicate how much each raster cell contributes to the nitrate mass in the

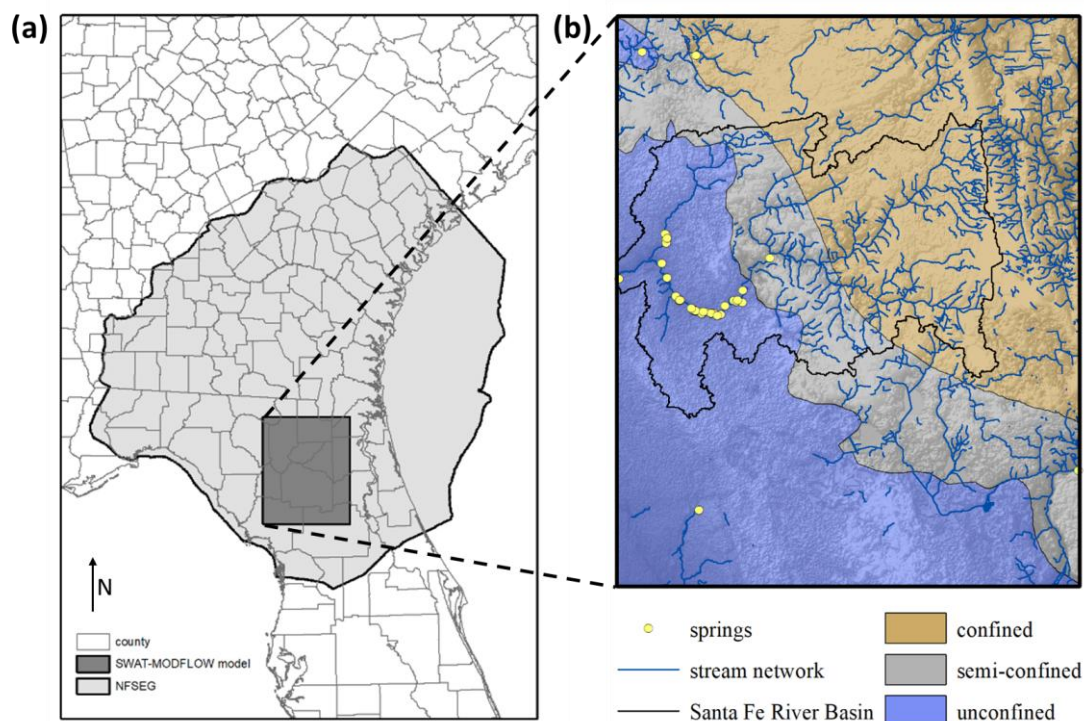


236 discharge area of interest. Nitrate mass contributions are mapped as a fraction of the total nitrate mass
237 discharged and thus also sum to unity. Together with the travel times the raster map of nitrate mass
238 contributions can be used to prioritize mitigation strategies for areas with higher contributions and shorter
239 travel times.

240 **3 Application of Modeling Framework**

241 **3.1 Santa Fe River Basin**

242 We applied the SWAT-MODFLOW and MODPATH modeling framework to the Santa Fe River Basin
243 (SFRB) in north-central Florida. Figure 3a illustrates the location and extent of our SWAT-MODFLOW
244 model of the SFRB. The degree of confinement of the Upper Floridan Aquifer (UFA) is mapped into
245 three distinct regions: a confined region, a semi-confined region, and an unconfined region (Figure 3b).
246 In the confined region, the UFA is overlain by the Intermediate Confining Unit (ICU) and the Surficial
247 Aquifer System (SAS). The confined region is dominated by surface water runoff, with abundant surface
248 drainage features including lakes, streams, and wetlands. In the unconfined region the ICU is absent, and
249 the limestone rocks of the UFA are overlain by a thin layer of sand (Arthur et al., 2005). The unconfined
250 region is dominated by groundwater flow and characterized by karst features such as sink holes and
251 springs and the absence of smaller streams feeding the main Santa Fe River (Hunn and Slack, 1983). The
252 UFA is underlain by the Middle Confining Unit (MCU) and the Lower Floridan Aquifer (LFA) (Williams
253 and Kuniatsky, 2015).



254

255 **Figure 3.** a) NFSEG and SWAT-MODFLOW Model domain locations in North Florida. b) Map
256 illustrating the extent of the confined, semi-confined and unconfined zone, stream network, the Santa Fe
257 River Basin and major springs in the SWAT-MODFLOW domain.

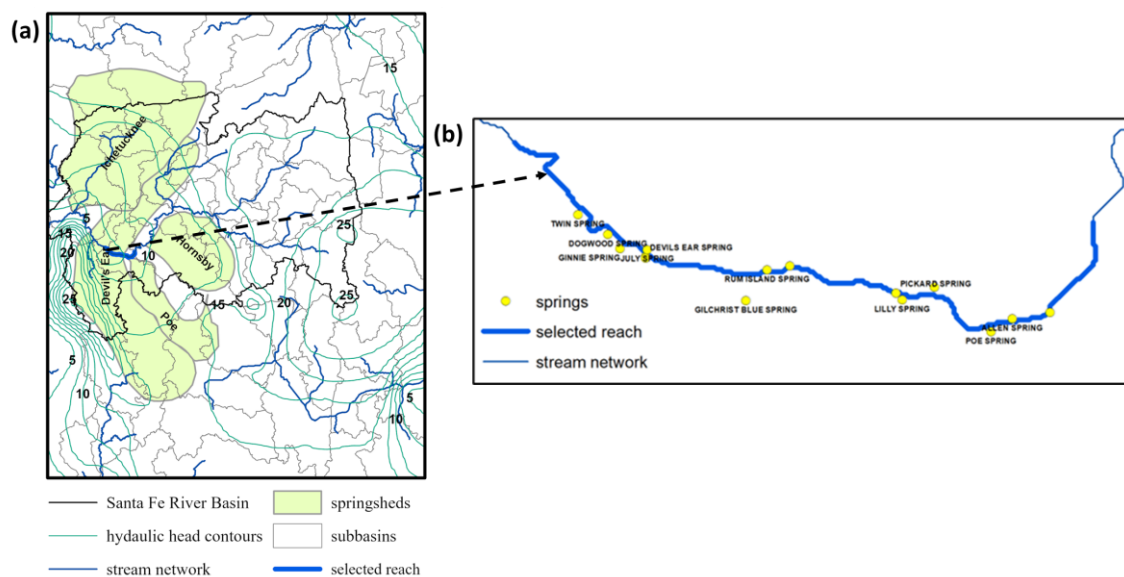
258

259 3.2 Model Setup

260 The MODFLOW model domain was clipped from the larger North Florida Southeast Georgia (NFSEG)
261 steady-state MODFLOW model (year 2001), developed by the St John’s River and Suwannee River
262 Water Management Districts (Durdan et al., 2019) . The extent of the NFSEG model is shown in Figure
263 3a. Natural flow boundaries to the Floridan Aquifer are not present in the close vicinity of the SFRB, so



264 to limit the size of the clipped model, we selected a rectangular model domain large enough to encompass
 265 the springsheds of several large springs along the Santa Fe River (Figure 4). Along the perimeter of the
 266 model, we applied fixed-head boundary conditions based on steady-state values of the NFSEG model.
 267 Pumping from municipal and domestic self-supply wells were taken from the NFSEG model.



268

269 **Figure 4.** a) Map of Santa Fe River subbasins, springsheds, stream network and springs within the SWAT-
 270 MODFLOW model domain. b) Springs along the selected river reach.

271

272 The NFSEG was developed as a steady-state model, however, SWAT-MODFLOW requires a transient
 273 MODFLOW model with specific storage coefficients. We assumed a value of $1E-4 \text{ m}^{-1}$ for all layers
 274 (Srivastava et al., 2014). Since the first layer is confined/unconfined, specific yields must also be defined,
 275 which we set to 0.25. Finally, we assumed porosity values of 0.25 throughout the model domain (Budd
 276 and Vacher, 2004). As discussed in Appendix B, reasonable travel times were only obtained after
 277 increasing the NFSEG Upper Floridan Aquifer horizontal hydraulic conductivity and decreasing the



278 NFSEG horizontal hydraulic conductivities in the Middle Confining Unit and the Lower Floridan Aquifer
279 to maintain the same effective horizontal conductivity across all layers.
280 While denitrification in the Floridan Aquifer is thought to be highly variably (Heffernan et al., 2012;
281 Henson et al., 2019; Yang et al., 2023), Heffernan et al. (2012) found an average 32% reduction in nitrate
282 in groundwater emerging from Upper Floridan Aquifer spring vents. Based on these studies we assumed
283 a first-order denitrification process with a half-life of 50 years which yields a 32% loss in groundwater
284 emerging from springs with a travel time of about 20 years, which is within the 16-27 year spring water
285 age estimated by Katz et al. (1999) and Katz (2004) using chlorofluorocarbon measurements. Previously
286 calibrated parameters governing denitrification in the SWAT domain were taken from (Rath, 2021).

287 **3.3 Intrinsic Vulnerability Land-Use Scenarios**

288 We used a sequence of three land-uses to explore intrinsic vulnerability and nitrate mitigation priorities
289 in the SFRB. The first land use (“pre-development”) mimics pre-development conditions. Until the end
290 of the 19th century, much of Florida remained undeveloped and low-density longleaf pines covered much
291 of the region (Volk et al., 2017). Around 1920, most of the old growth forests were logged and converted
292 to higher density production forestry or agriculture. Thus, for the pre-development land use we replaced
293 all current agricultural and forestry lands with low-density longleaf pine and replaced all current rural
294 area and urban areas with grasslands. Moreover, in this scenario there was no groundwater pumping for
295 municipal use, agriculture or domestic self-supply and no wastewater effluent discharge from septic tanks
296 or wastewater treatment plants. The second land use (“current conditions”, Figure 5) represents the current
297 land use of the study region derived from the Statewide Land Use / Land Cover map of the Florida



298 Department of Environmental protection (FDEP) for the year 2017 with water, nutrient and other
299 residential, agricultural and silvicultural management practices defined through a stakeholder engagement
300 process (Bartels and Furman, 2023). Pumping from municipal and domestic self-supply wells was taken
301 from the NFSEG model and nitrate loading from septic tanks and wastewater effluent disposal, as well as
302 fertilizer usage on agricultural, silvicultural and residential lands, was simulated by SWAT. The third
303 land use (“restoration forestry”) represents a scenario in which all current agricultural and forestry lands
304 are replaced with low-density longleaf pines, but rural residential and urban land uses remain. The
305 SWAT-MODFLOW model with current land use conditions was calibrated to stream flows at USGS
306 gauge stations in the Santa Fe River, hydraulic head contour maps (Fdep, 2023) and remote sensing
307 estimates of evapotranspiration (Senay and Kagone, 2019) using NLDAS weather data from 1980 to
308 2018. During the calibration period (2010-2018), the Nash–Sutcliffe efficiency (NSE) was 0.68 for daily
309 streamflow at the Ft. White gauging station (station ID 02322500), and overall groundwater elevation and
310 ET NSE values were of 0.70 and 0.83, respectively. For the validation period (1980-2009), NSE was 0.45
311 for daily streamflow and overall NSE for ET was 0.82. Details regarding SWAT-MODFLOW model
312 development and calibration for the SFRB are documented and available as a CUAHSI HydroShare
313 (Reaver et al., 2025).

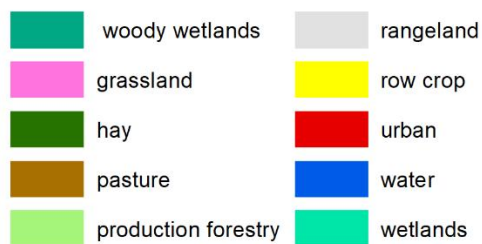
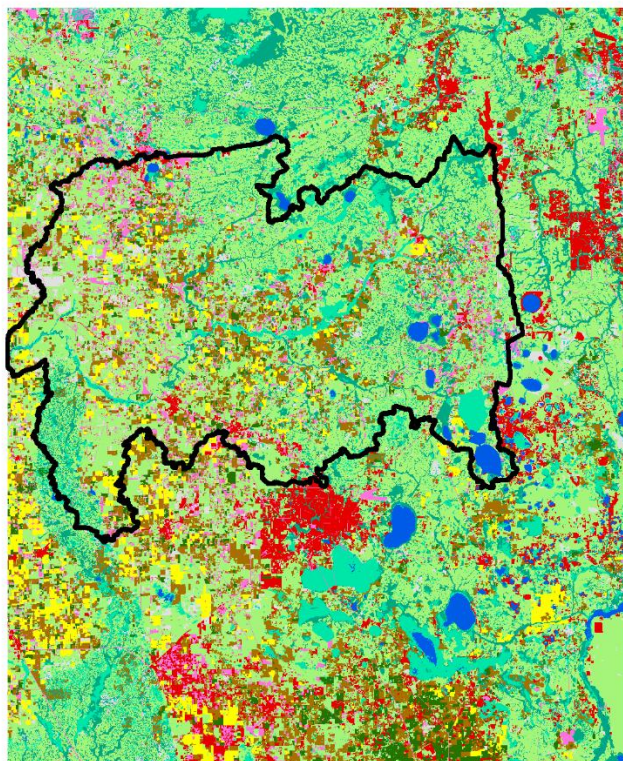
314 Using the three land use periods, we constructed a stand-alone MODFLOW model with three steady-state
315 stress periods (pre-development, followed by current conditions, followed by restoration forestry) using
316 the averaged boundary conditions from each model that was run from 1980 to 2018. Since the flow field
317 changed between stress periods, the particle-tracking results depend on the time of release. To simulate
318 the long-term effects of a future land use based on restoration forestry, the third period was set to 100



319 years. The length of the second period was 80 years such that if we release particles at the end of this
320 period, we will simulate results for the present. We thus assume that current land use and management
321 practices go back 80 years. The first period extended as long as necessary for MODPATH to back-track
322 particles to reach their aquifer entry point. Each particle-tracking simulation was carried out with a million
323 particles.

324 After construction of the stand-alone MODFLOW model, we back-tracked particles from a Sante Fe
325 River reach containing a large number of first- and second-order magnitude springs including Ginnie
326 Spring, July Spring, Devil's Ear Spring, Gilchrist Blue Spring, Rum Island Spring and Poe Spring (Figure
327 4b). All of these springs are classified as impaired, with Nitrate-Nitrogen (NO₃-N) concentrations ranging
328 from 1.5 to 6 times above the Numeric Nutrient Criteria (NNC) of 0.35 mg/l NO₃-N (Fdep, 2018). As a
329 result, state regulations mandate the establishment of a Basin Management Action Plan (BMAP) designed
330 to reduce nitrate loadings and achieve the NNC within 20 years.

331



332

333 **Figure 5.** Land use map for current conditions within the SWAT-MODFLOW domain.

334

335 After observing the travel times and nitrate load contributions to this river reach for the current land use
336 conditions and the response to conversion to restoration forestry across the entire domain, we simulated
337 a targeted nitrate load mitigation strategy. This strategy included the removal of all septic tanks and
338 fertilized lawns and the conversion of all agricultural lands within a 30-year travel time contour to



339 restoration forestry. For this simulation we did not simulate an additional scenario with a separate SWAT-
340 MODFLOW model. Instead, we derive the last stress period from the existing three scenarios. Namely,
341 we replaced the agricultural HRU values for percolation and nitrate loading within the 30-year travel time
342 contour with corresponding HRU values from the restoration forestry scenario and reduced the amount
343 of pumping needed for agriculture accordingly. We also replaced the HRU values for percolation and
344 nitrate loading from septic tanks and rural areas with the corresponding the grassland values from the pre-
345 development scenario. Finally, using the relationship between SWAT HRUs and MODFLOW raster cells
346 as discussed in section 2.5, we computed the average boundary conditions for the third period in our
347 stand-alone MODFLOW model. Exchanging HRU values between different scenarios is valid because in
348 SWAT-MODFLOW the computations on the HRUs are independent of the MODFLOW computations.
349 Since this methodology avoids the need for running a separate SWAT-MODFLOW model, it is more
350 efficient.

351

352 **4 Results**

353 **4.1 Groundwater and Nitrate Travel Time Distributions**

354 Figure 6a illustrates the travel time distributions (TTDs) for current conditions ($t=80$ years). After
355 parameter modifications detailed in Appendix B, the median water travel time for the current condition
356 scenario is about 32 years, which corresponds reasonably well with age values of 16-27 years derived
357 from chlorofluorocarbons measurements (Katz et al., 1999). Figure 6b illustrates the TTDs of the
358 corresponding nitrate mass based on the assumed half-life of 50 years. The median nitrate mass age of 19

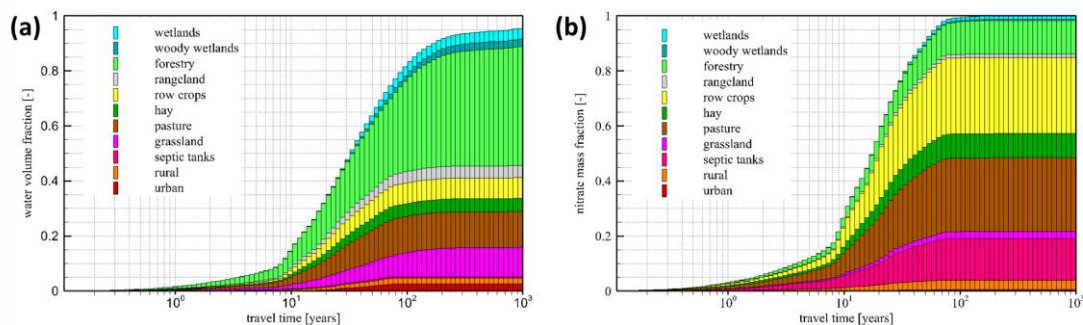


359 years is lower than the median water age. It is noted the difference in TTD's between water volumes and
360 nitrate masses is not only caused by denitrification but also by differences in the source areas between the
361 water volumes and the nitrate masses.

362 Since each back-tracked particle comes from a specific land use, we can partition the areas below the
363 TTDs according to cumulative land use fractions as illustrated in Figure 6a and 6b. In the current
364 condition, production forestry is the land use that contributes the largest volume of discharged water (Fig.
365 6a), whereas row crops, pasture, and septic tanks contribute the largest nitrate mass (Fig. 6b). Rural and
366 urban lands also contribute to the nitrate mass due to fertilized lawns. We can also construct TTDs for
367 each source component separately (Fig. 7a), illustrating that certain source components have a maximum
368 age of 80 years; these components are associated with land use types that did not exist during pre-
369 development conditions.

370 Figure 7b illustrates how the concentration of nitrate in the discharged groundwater changes with time
371 over the three scenario periods, partitioned according to source components. As expected, the
372 concentration of nitrate increases after switching from pre-development to current conditions and
373 decreases after the switch to restoration forestry. The lag between changes in nitrate loading and nitrate
374 concentration in discharged water is a consequence of groundwater travel times. The NNC is achieved
375 approximately 60 years after the switch to restoration forestry.

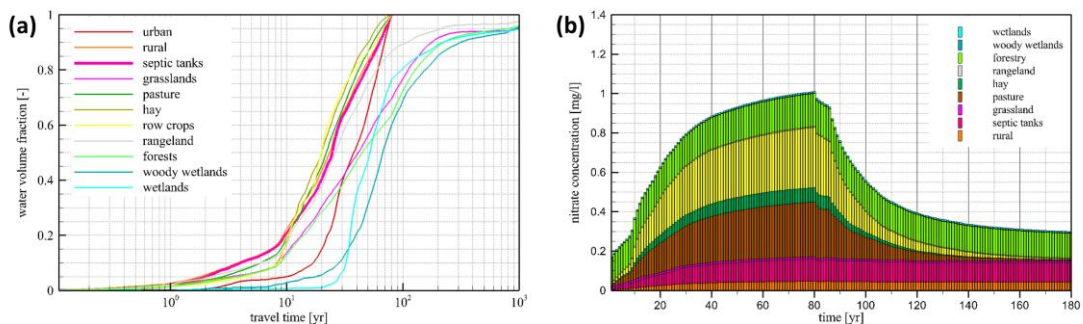
376



377

378 **Figure 6.** Travel time CDF of water volumes (a) and nitrate masses (b) within the selected river reach
 379 with source components for the current conditions.

380



381

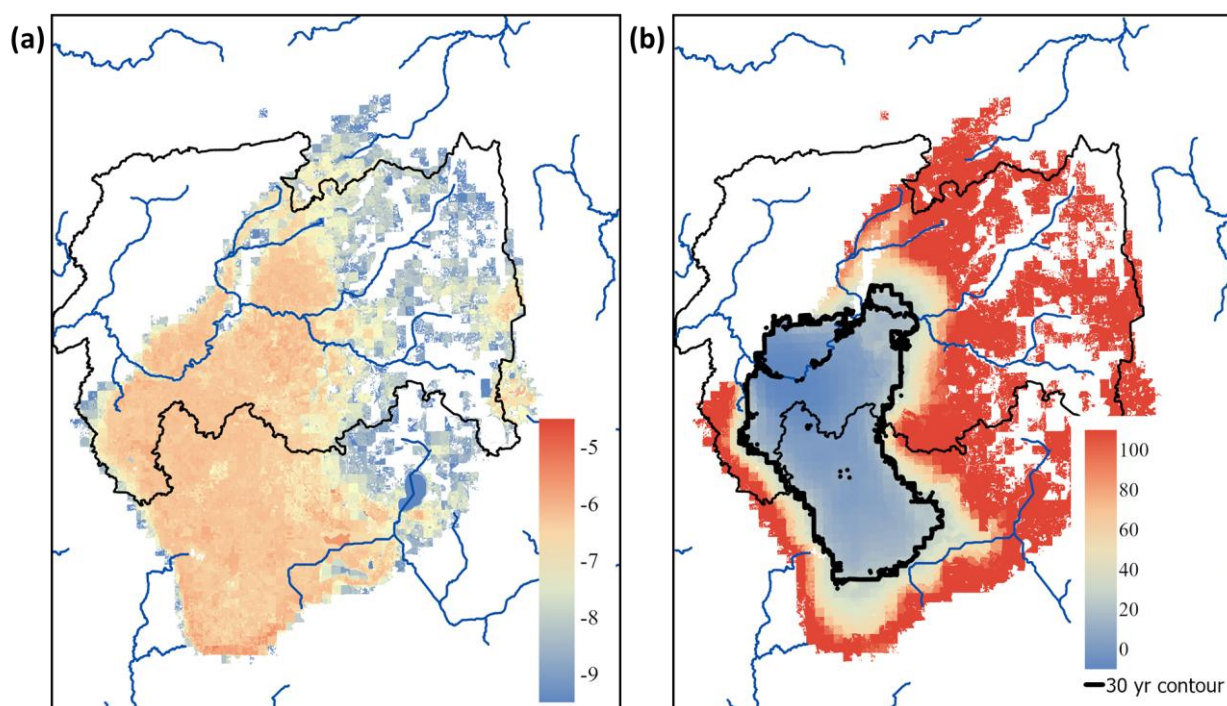
382 **Figure 7.** a) Travel time CDF's of water volumes per source component and b) Nitrate concentration in
 383 discharged groundwater as a function of time assuming transition from predevelopment conditions to
 384 current conditions at year 0 and transition from current conditions to restoration forestry at year 80.

385 **4.2 Intrinsic Vulnerability and Mitigation Prioritization**

386 Figure 8a and 8b show maps of the fraction of particles back-tracked to the source areas and the average
 387 travel time, respectively. These maps are for particles released at the end of the current condition period,



388 just before the switch to restoration forestry. Since each particle represents an equal volume of water, a
389 higher fraction of particles represents a higher contribution to the discharge volume. These maps are
390 important qualitative indicators for intrinsic vulnerability. Namely areas with high particle fractions and
391 low travel times are most vulnerable to contaminants as these areas would contribute relatively quickly
392 and significantly to the contaminant concentration in the discharge area.



393

394 **Figure 8.** a) Map of water volume fractions back-tracked to the source areas (log scale) and b) Travel
395 time map (in years) for current condition.

396

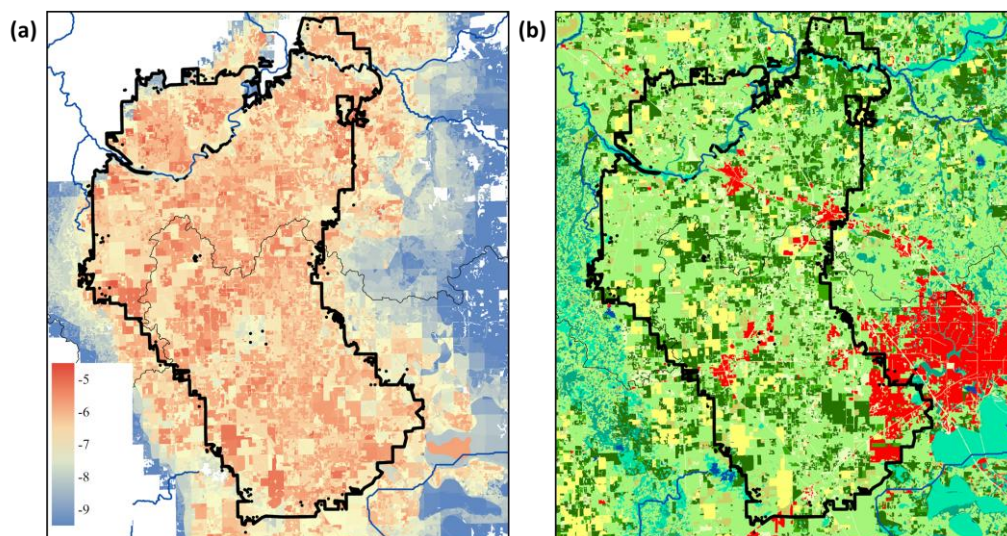
397 Since we have the nitrate loadings from the SWAT model, we can compute how much each particle
398 contributes to the total concentration in the discharged groundwater, which provides insights into which
399 areas contribute the most to the nitrate concentrations in discharged groundwater. This is illustrated in



400 Figure 9a for particles released at the end of the current condition period. Similar to the results shown in
401 Figure 7b, Figure 9a and 9b indicate that agriculture is the largest contributor to nitrate concentrations,
402 since the most significant contribution areas correspond to agricultural land uses. Together with the travel
403 time map in Figure 8b, the map of mass contributions may be used to design potential mitigation
404 strategies.

405 A potential mitigation strategy that results in meeting the mandated reduction to the NNC more quickly
406 and with less land use change than the full restoration forestry scenario is to remove all septic tanks and
407 fertilized lawns within rural lands and to convert all agriculture land uses within the travel time contour
408 of 30 years into restoration forestry. The decrease in nitrate concentration with time due to this mitigation
409 strategy is shown in Figure 10. In this case the NNC is achieved after 50 years, and 163507 hectares of
410 the current condition 196315 hectares of agriculture remain in production contributing to the regional
411 economy.

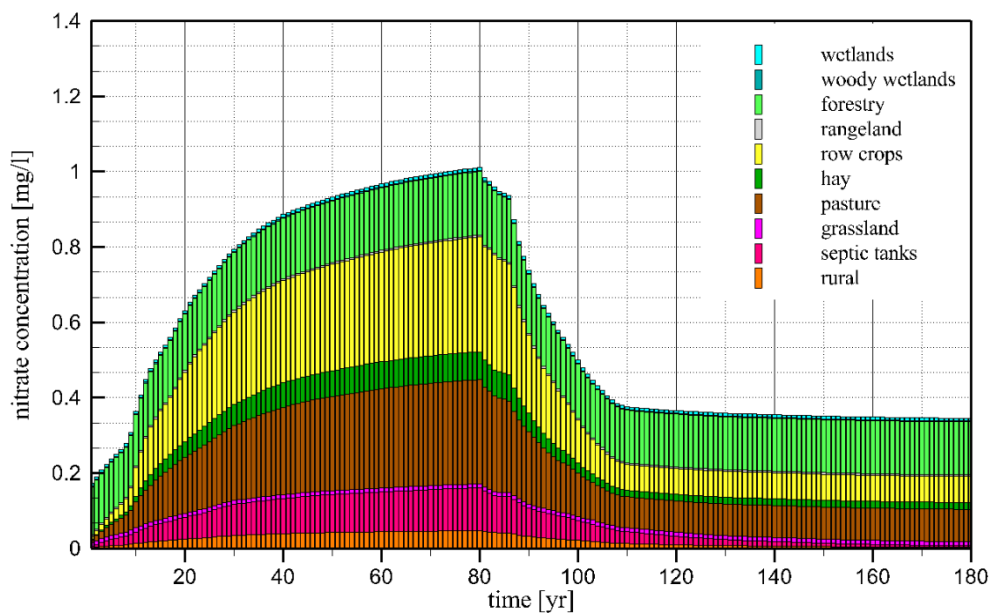
412



413



414 **Figure 9.** a) Map of nitrate mass fraction back-tracked to the source areas (log scale) and b) Land use
415 map (see Figure 5 for legend) for current condition.



416
417 **Figure 10.** Nitrate concentration in discharged groundwater as a function of time for targeted restoration
418 which 1) replaces agricultural and production forestry within the 30 years travel time contour with
419 restoration forestry and 2) removes all septic tanks and replaces fertilized rural lawns with unfertilized
420 grassland.

421 5 Discussion

422 Numerical models have been widely recognized as useful tools to assess the fate and transport of nitrate
423 in groundwater (Rawat et al., 2022). The recently developed SWAT-MODFLOW-RT3D code (Wei et
424 al., 2019), is a particularly useful numerical simulation tool since nitrate loading to the groundwater



425 domain can be simulated for different land use and climate scenarios (Wei et al., 2019). In this study, we
426 propose an alternative novel modeling framework. Instead of simulating transport in the groundwater
427 domain by means of an advection-dispersion-reaction equation as in SWAT-MODFLOW-RT3D, we
428 simulate transport by backward particle-tracking using SWAT-MODFLOW and MODPATH. This idea
429 is motivated by a range of other studies that have shown that particle-tracking is a useful tool to gain
430 insights into the source areas and travel times of groundwater (Engdahl et al., 2016; Kaandorp et al., 2018;
431 Maxwell et al., 2019; Wilusz et al., 2020) and into the intrinsic vulnerability of groundwater systems
432 (Medici et al., 2021; Molson and Frind, 2012). Whereas particle-tracking to simulate nitrate transport
433 typically requires an explicit boundary condition for nitrate mass loading (Kaandorp et al., 2021;
434 Mullaney, 2007; Kauffman, 2001), SWAT-MODFLOW provides this loading as a function as weather,
435 soil and hydrologic conditions, land use and management within our coupled modeling framework.

436 **5.1 Framework Application and Advantages**

437 We applied our modeling framework to a river reach in the Santa Fe River Basin in north-central Florida
438 which is fed by a large number of first and second magnitude springs that are impaired by elevated nitrate
439 concentrations. Initial application of our modeling approach to simulate the age and source components
440 for water volumes in this reach provided useful insights into the underlying flow model which resulted in
441 significant changes to the calibrated model parameters (see Appendix B for details). After these
442 modifications we simulated a median groundwater travel time of about 30 years (Figure 6) which
443 corresponds well with values of 16-27 years as derived from chlorofluorocarbons measurements (Katz et
444 al., 1999). TTDs can be constructed for groundwater volumes as well as nitrate masses. Using the source



445 components of the particles the simulated TTDs can be portioned according to land use type (Figure 7)
446 or separate TTDs can be constructed for each land use separately (Figure 8a).
447 Our modeling framework can account for changes in land use over time. By back-tracking particles at
448 different times and using different nitrate loading maps, we can simulate the change in groundwater nitrate
449 concentrations in a discharge zone of interest as a function of time. In our model application, we show
450 that there is a significant lag time between a change in nitrate loading and the subsequent reduction in
451 nitrate concentrations at the springs (Figure 8b). This lag time is a direct result of the travel time
452 distribution of discharged water. An understanding of this lag time is imperative for sustaining consensus
453 within communities with respect to mitigation efforts. Specifically, if the lag is not well understood,
454 delays in water quality improvement may erroneously be attributed to an improper mitigation plan. The
455 final locations of the back-tracked particles can be used to establish water and nitrate source density maps
456 by counting the number of these locations on a user-defined raster. The particle density on such maps
457 (Figure 8a) indicate how much different areas contribute to groundwater discharge. Together with the
458 travel time maps (Figure 8b) these density maps are indicative of intrinsic vulnerability. However, since
459 we have the simulated nitrate loadings, we can go further and establish maps indicating the nitrate mass
460 contributions for different areas (Figure 9a). These contributions together with the travel time map are of
461 direct use for prioritizing mitigation strategies. In this study, we show an example of a mitigation strategy
462 based on targeting those areas which contribute most significantly to the nitrate discharge. Our modeling
463 framework permits us to simulate the effect of this mitigation strategy in terms of a change of nitrate
464 concentrations in discharged groundwater as a function of time (Figure 10). Results indicate that the
465 mandated reduction to the NNC of 0.35 mg/l NO₃-N within 20 years may not be realistic. If all



466 agricultural lands (196315 hectares) and forestry (561904 hectares) are replaced with low-density longleaf
467 pines, our simulation results indicate that reaching the NNC takes about 60 years. If all agricultural lands
468 within the 30-year travel time contour are replaced with low-density longleaf pines (32808 hectares), all
469 septic tanks are removed, and all lawn fertilization in rural areas is eliminated it takes about 50 years to
470 reach the NNC.

471 With respect to SWAT-MODFLOW-RT3D, our modeling framework retains the feature that nitrate
472 loadings to the groundwater domain can be simulated as a function of land use and weather conditions.
473 Contrary to SWAT-MODFLOW-RT3D which can simulate the nitrate concentrations in the entire
474 SWAT-MODFLOW domain, our modeling approach only simulates nitrate concentrations in particular
475 groundwater discharge zones of interest. However, in terms of designing mitigation strategies, our
476 modeling framework offers a clear advantage as it provides the source and age components needed to
477 guide optimal water quality improvement strategies.

478 **5.2 Limitations and Uncertainties**

479 It is important to highlight assumptions made in this study that may limit our findings. The particle-
480 tracking results, and thus the simulated TTDs and nitrate concentrations, depend on the flow fields as
481 simulated by the SWAT-MODFLOW models. In this study we use the equivalent porous medium concept
482 model to a groundwater system characterized by numerous karstic features. Our modeling approach
483 makes simplifying assumptions regarding historical and current land use and assumes that the effective
484 recharge and nitrate loading to MODFLOW are reasonably well simulated by SWAT-MODFLOW.
485 Travel times are only determined for the saturated portion of the MODFLOW domain and do not account



486 for travel times through dry MODFLOW cells or the soil layers in SWAT. The application of MODPATH
487 also requires the assumption that reasonable porosity values can be specified and that nitrate transport is
488 purely advective without dispersion. Finally, travel times for nitrate masses as well as simulated nitrate
489 concentrations depend on the assumed denitrification processes and parameters. Possibilities for
490 improving on these assumptions should be investigated in future work. With regard to our Santa Fe River
491 Basin models, future explorations into model equifinality and uncertainty would be useful. For example,
492 in this study we only use a single set of model parameters for the groundwater domain. The uncertainty
493 about these parameters is high, especially within the Upper Floridan Aquifer, due to the presence of
494 karstic voids related to the dissolution of carbonate rocks. In fact, it is reasonable to question the validity
495 of using a single equivalent porous medium layer for this aquifer. However, when using SWAT-
496 MODFLOW alternative representations for the Upper Floridan Aquifer are limited. SWAT-MODFLOW
497 cannot handle turbulent flow in karstic conduits. Moreover, little information exists about the location
498 and geometry of karstic conduits. Nonetheless, alternative representations within the limitations of
499 SWAT-MODFLOW may be possible. For example, the aquifer could be divided into a number of separate
500 layers of porous medium types. By doing so, the duality of flow regimes within the aquifer could be
501 represented; slower flow in the porous limestone matrix and faster albeit laminar flow in karstified
502 horizons. Regardless of representation, however, the uncertainty about the model parameters can only be
503 accounted for by running multiple model realizations. Likewise, we acknowledge that we did not explore
504 the sensitivity of the model parameters that govern the denitrification processes.



505 **6 Conclusions**

506 This study presents a modeling framework that integrates MODPATH with SWAT-MODFLOW to
507 simulate groundwater nitrate transport in terms of source areas and travel time distributions. By
508 combining backward particle tracking with nitrate loading simulated by SWAT, the approach provides a
509 computationally efficient alternative to fully coupled reactive transport models. Application of the
510 framework to the Santa Fe River Basin demonstrates its effectiveness. Results show that groundwater
511 travel time distributions strongly control nitrate delivery to spring-fed river reaches. Simulated travel
512 times have a median on the order of three decades, indicating substantial lag times between reductions in
513 nitrate loading and measurable improvements in water quality.

514 In addition to simulating nitrate concentrations at locations of interest, the framework spatially identifies
515 the source areas and travel times that govern nitrate delivery. Linking particle source locations with
516 simulated nitrate loading enables mapping of nitrate contributions from different land uses and
517 quantifying their relative influence on concentrations in groundwater. Results show that mitigation
518 strategies focused on source areas with shorter travel times reduce nitrate concentrations more efficiently
519 than uniform basin-wide land-use changes, although improvements may still occur over multi-decadal
520 time scales due to subsurface transport lags. By explicitly resolving both the age and source components
521 of nitrate transport, the proposed framework provides a practical and transferable tool for prioritizing
522 water quality mitigation strategies in groundwater-dominated watersheds.

523

524

525



526 **Appendix A**

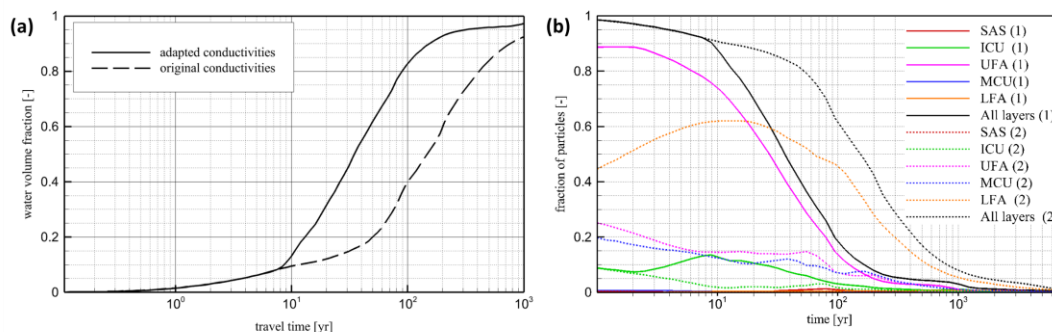
527 For this study, we made a significant change to the current SWAT-MODFLOW Version 3 code
528 (<https://swat.tamu.edu/software/swat-modflow/>) regarding the water stages in the river. The original
529 SWAT-MODFLOW code is designed with the intention that the reach water stages as computed by
530 SWAT are used as river stages by MODFLOW. However, in the current SWAT-MODFLOW code, the
531 reach stages are not transferred correctly to corresponding river cells. A river cell may be connected to
532 one or more reaches. At a junction of reaches, for example, a cell can be connected to three reaches. To
533 set the river stage in such a cell, the intention is to find a weighted average of the water depths in the
534 reaches based on their length within the river cell. In the part of the code where this is supposed to be
535 computed, however, the computation is incomplete and thus incorrect. For each cell the code finds the
536 number m , where m is the number of reaches connected to the river cell. This cell is then connected to
537 reaches 1 to m . However, these numbers are not the actual reach numbers to which the cell needs to be
538 connected. After we corrected this coupling issue using the correct reach numbers, however, the river
539 stages became highly oscillatory as a result of the sequential non-iterative coupling between SWAT and
540 MODFLOW. Basically, the water stages are transferred without any further communication between the
541 models during the time step. It is worthwhile to mention that GSFLOW (Markstrom et al., 2008), another
542 model for coupling surface and subsurface flow, uses a sequential iterative approach which is more robust.
543 Here, we circumvent the instability problem, by setting the river stages in MODFLOW equal to the river
544 bottom. This implies that the river exchange flux between SWAT and MODFLOW becomes independent
545 on the reach stages as computed by SWAT. It can be argued that this is reasonable except during periods
546 with relatively extreme variations in the reach stages.



547

548 **Appendix B**

549 As mentioned in section 3.2, reasonable travel times are only obtained when we increase the horizontal
550 hydraulic conductivity in the Upper Floridan Aquifer and decrease the horizontal hydraulic conductivity
551 in the Middle Confining Unit and the Lower Floridan Aquifer with respect to the original values in the
552 NFSEG model. To illustrate this in more detail, we run a stand-alone model with the original NFSEG
553 hydraulic conductivity values for the current conditions. Figure B1 shows the TTD for water volumes and
554 indicates the median travel time using the original hydraulic conductivity values is about 150 years. This
555 result does not correspond well with values obtained from CFC measurements (Katz et al., 1999). Upon
556 closer examination of the particle-tracking results, (Figure A1b) it is observed that many particles move
557 through the Lower Floridan aquifer. Contrary to this simulated result the water discharged at the springs
558 is believed to travel mainly through the Upper Floridan Aquifer since it has been subjected more to
559 karstification than the Lower Floridan Aquifer, especially in the unconfined zones (Williams and
560 Kuniansky, 2015). To force more flow through the Upper Floridan Aquifer and obtain reasonable travel
561 times we decrease the horizontal hydraulic conductivity of the Lower Floridan Aquifer and Middle
562 Confining Unit by a factor of 100 and increase the horizontal hydraulic conductivity of the Upper Floridan
563 such that the equivalent horizontal hydraulic conductivity of all three layers remains the same. As a result,
564 our new model and the original model yield similar hydraulic head fields. This is important since the
565 NFSEG is calibrated to hydraulic heads.



566

567 **Figure B1.** a) Travel time CDF's using original and adapted horizontal conductivities and b) Fraction of
568 particles (with respect to total number of released particles) in each layer as a function of time for original
569 conductivities (solid lines, 1) and adapted conductivities (dashed lines 2).

570

571 Code and data availability

572 The SWAT-MODFLOW model used in this study is available as a CUAHSI HydroShare (Reaver et al.,
573 2025).

574 Author contributions

575

576 RdR: conceptualization, methodology, software, data curation, formal analysis, validation, visualization,
577 writing (original draft); NR: methodology, data curation, formal analysis, validation, writing (review and
578 editing); DL: methodology, software, formal analysis, validation, DK: conceptualization, methodology,
579 formal analysis, validation, funding acquisition, supervision, writing (review and editing), and WG



580 conceptualization, methodology, formal analysis, validation, funding acquisition, project administration,
581 supervision, writing (review and editing).

582 **Competing interests**

583 The authors declare there are no conflicts of interest for this manuscript.

584 **Financial support**

585 This work was supported in part by the U.S. Department of Agriculture National Institute of Food and
586 Agriculture (award number 2017-68007-26319). and the Carl S. Swisher Foundation. The findings and
587 conclusions in this manuscript are those of the authors and should not be construed to represent any
588 official USDA or U.S. Government determination or policy.

589

590 **References**

- 591 Arnold, J. G., Srinivasan, R., Muttiah, R. S., and Williams, J. R.: Large area hydrologic modeling and assessment - Part 1:
592 Model development, *Journal of the American Water Resources Association*, 34, 73-89, 10.1111/j.1752-
593 1688.1998.tb05961.x, 1998.
- 594 Arthur, J. D., Baker, A. E., Cichon, J. R., Wood, A. R., and Rudin, A.: Florida Aquifer Vulnerability Assessment (FAVA):
595 Contamination potential of Florida's principal aquifer systems, Report submitted to the Division of Water Resource
596 Management, Florida Department of Environmental Protection. Tallahassee: Division of Resource Assessment and
597 Management, Florida Geological Survey, 2005.
- 598 Bailey, R. T., Wible, T. C., Arabi, M., Records, R. M., and Ditty, J.: Assessing regional-scale spatio-temporal patterns of
599 groundwater-surface water interactions using a coupled SWAT-MODFLOW model, *Hydrological Processes*, 30, 4420-4433,
600 10.1002/hyp.10933, 2016.
- 601 Bartels, W.-L. and Furman, C. A.: Building community for participatory modeling: network composition, trust, and adaptive
602 process design, *Society & Natural Resources*, 36, 326-346, 2023.
- 603 Benettin, P., Rodriguez, N. B., Sprenger, M., Kim, M., Klaus, J., Harman, C. J., Van Der Velde, Y., Hrachowitz, M., Botter,
604 G., and McGuire, K. J.: Transit time estimation in catchments: Recent developments and future directions, *Water Resources
605 Research*, 58, e2022WR033096, 2022.



- 606 Budd, D. A. and Vacher, H.: Matrix permeability of the confined Floridan Aquifer, Florida, USA, *Hydrogeology Journal*, 12,
607 531-549, 2004.
- 608 De Rooij, R., Graham, W., and Maxwell, R.: A particle-tracking scheme for simulating pathlines in coupled surface-
609 subsurface flows, *Advances in Water Resources*, 10.1016/j.advwatres.2012.07.022, 2012.
- 610 Durden, D., Gordu, F., Hearn, D., Cera, T., Desmarais, T., Meridith, L., Angel, A., Leahy, C., Oseguera, J., Grubbs, T.,
611 Meridith, L., Angel, A., and Grubbs, T.: North Florida southeast Georgia groundwater model (NFSEG V1. 1), St Johns River
612 Management District, Palatka, Florida, 2019.
- 613 Engdahl, N. B., McCallum, J. L., and Massoudieh, A.: Transient age distributions in subsurface hydrologic systems, *Journal*
614 *of Hydrology*, 543, 88-100, 2016.
- 615 FDEP: Santa Fe River Basin management Action Plan, Division of Environmental Assessment and Restoration, Water
616 Quality Restoration Program, Florida Department of Environmental Protection, Tallahassee, Florida, 2018.
- 617 FDEP: Upper Floridan Aquifer Potentiometric Surface. In "Florida Department of Environmental Protection Geospatial
618 Open Data". 2023.
- 619 Harbaugh, A. W.: MODFLOW-2005, the US Geological Survey modular ground-water model: the ground-water flow
620 process, US Department of the Interior, US Geological Survey Reston, VA2005.
- 621 Heffernan, J., Albertin, A., Fork, M., Katz, B., and Cohen, M.: Denitrification and inference of nitrogen sources in the
622 karstic Floridan Aquifer, *Biogeosciences*, 9, 1671-1690, 2012.
- 623 Henson, W. R., Cohen, M. J., and Graham, W. D.: Spatially distributed denitrification in a karst springshed, *Hydrological*
624 *Processes*, 33, 1191-1203, 2019.
- 625 Hunn, J. D. and Slack, L. J.: Water resources of the Santa Fe river basin, Florida, US Geological Survey, 1983.
- 626 Kaandorp, V., De Louw, P., Van der Velde, Y., and Broers, H.: Transient groundwater travel time distributions and age-
627 ranked storage-discharge relationships of three lowland catchments, *Water Resources Research*, 54, 4519-4536, 2018.
- 628 Kaandorp, V. P., Broers, H. P., Van Der Velde, Y., Rozemeijer, J., and De Louw, P. G.: Time lags of nitrate, chloride, and
629 tritium in streams assessed by dynamic groundwater flow tracking in a lowland landscape, *Hydrology and Earth System*
630 *Sciences*, 25, 3691-3711, 2021.
- 631 Katz, B., Hornsby, D., Bohlke, F., and Mokray, M.: Sources and chronology of nitrate contamination in spring waters,
632 Suwannee River Basin, Florida. Water-Resources Investigations Rep. 99-4252, Tallahassee. FLU. S. Geological Survey,
633 1999.
- 634 Kauffman, L. J.: Effects of land use and travel time on the distribution of nitrate in the Kirkwood-Cohansey aquifer system
635 in southern New Jersey, 1, US Department of the Interior, US Geological Survey2001.
- 636 Markstrom, S. L., Niswonger, R. G., Regan, R. S., Prudic, D. E., and Barlow, P. M.: GSFLOW-Coupled Ground-water and
637 Surface-water FLOW model based on the integration of the Precipitation-Runoff Modeling System (PRMS) and the Modular
638 Ground-Water Flow Model (MODFLOW-2005), *US Geological Survey techniques and methods*, 6, 240, 2008.
- 639 Maxwell, R. M., Condon, L. E., Danesh-Yazdi, M., and Bearup, L. A.: Exploring source water mixing and transient
640 residence time distributions of outflow and evapotranspiration with an integrated hydrologic model and Lagrangian particle
641 tracking approach, *Ecohydrology*, 12, e2042, 2019.
- 642 Medici, G., Engdahl, N. B., and Langman, J. B.: A basin-scale groundwater flow model of the Columbia Plateau regional
643 aquifer system in the Palouse (USA): Insights for aquifer vulnerability assessment, *International Journal of Environmental*
644 *Research*, 15, 299-312, 2021.
- 645 Molson, J. W. and Frind, E. O.: On the use of mean groundwater age, life expectancy and capture probability for defining
646 aquifer vulnerability and time-of-travel zones for source water protection, *Journal of Contaminant Hydrology*, 127, 76-87,
647 10.1016/j.jconhyd.2011.06.001, 2012.
- 648 Mullaney, J. R.: Nutrient loads and ground-water residence times in an agricultural basin in north-central Connecticut2328-
649 0328, 2007.
- 650 Niswonger, R. G., Panday, S., and Ibaraki, M.: MODFLOW-NWT, a Newton formulation for MODFLOW-2005, *US*
651 *Geological Survey Techniques and Methods*, 6, 44, 2011.
- 652 Pan, L. and Bodvarsson, G. S.: Modeling transport in fractured porous media with the random-walk particle method: The
653 transient activity range and the particle transfer probability, *Water Resources Research*, 38, 16-11-16-17, 2002.
- 654 Park, S. and Bailey, R.: SWAT-MODFLOW Tutorial—Documentation for Preparing Model Simulations, Department of
655 Civil and Environmental Engineering, Colorado State University: Fort Collins, CO, USA, 2017.



- 656 Park, S., Nielsen, A., Bailey, R. T., Trolle, D., and Bieger, K.: A QGIS-based graphical user interface for application and
657 evaluation of SWAT-MODFLOW models, *Environmental Modelling & Software*, 111, 493-497,
658 10.1016/j.envsoft.2018.10.017, 2019.
- 659 Pollock, D. W.: User guide for MODPATH Version 7—A particle-tracking model for MODFLOW, US Geological
660 Survey2331-1258, 2016.
- 661 Rath, S.: Agricultural water security through sustainable use of the Floridan aquifer: An integrated study of water quantity
662 and water quality impacts, University of Florida, 2021.
- 663 Rawat, M., Sen, R., Onyekwelu, I., Wiederstein, T., and Sharda, V.: Modeling of groundwater nitrate contamination due to
664 agricultural activities—a systematic review, *Water*, 14, 4008, 2022.
- 665 Reaver, N. G. F., Lee, D., Rooij, R. D., Kaplan, D., and Graham, W.: The Floridan Aquifer Collaborative Engagement for
666 Sustainability
(FACETS) project SWAT-MODFLOW model of the Santa Fe River, Florida [dataset], 2025.
- 667 Rodriguez, N. B., Pfister, L., Zehe, E., and Klaus, J.: A comparison of catchment travel times and storage deduced from
668 deuterium and tritium tracers using StorAge Selection functions, *Hydrology and Earth System Sciences*, 25, 401-428, 2021.
- 669 Senay, G. and Kagone, S.: Daily SSEBop evapotranspiration data from 2000 to 2018, US Geological Survey (USGS) Data
670 Release, 931, 2019.
- 672 Srivastava, V., Graham, W., Munoz-Carpena, R., and Maxwell, R. M.: Insights on geologic and vegetative controls over
673 hydrologic behavior of a large complex basin - Global Sensitivity Analysis of an integrated parallel hydrologic model,
674 *Journal of Hydrology*, 519, 2238-2257, 10.1016/j.jhydrol.2014.10.020, 2014.
- 675 Visser, A., Heerdink, R., Broers, H., and Bierkens, M.: Travel time distributions derived from particle tracking in models
676 containing weak sinks, *Groundwater*, 47, 237-245, 2009.
- 677 Volk, M. I., Hocht, T. S., Nettles, B. B., Hilsenbeck, R., Putz, F. E., and Oetting, J.: Florida land use and land cover change
678 in the past 100 years, *Florida's Climate: Changes, Variations, & Impacts*, 2017.
- 679 Wei, X., Bailey, R. T., Records, R. M., Wible, T. C., and Arabi, M.: Comprehensive simulation of nitrate transport in
680 coupled surface-subsurface hydrologic systems using the linked SWAT-MODFLOW-RT3D model, *Environmental
681 Modelling & Software*, 122, 104242, 2019.
- 682 Williams, L. J. and Kuniandy, E. L.: Revised hydrogeologic framework of the Floridan aquifer system in Florida and parts
683 of Georgia, Alabama, and South Carolina, US Geological Survey2330-7102, 2015.
- 684 Wilusz, D., Harman, C., Ball, W., Maxwell, R., and Buda, A.: Using particle tracking to understand flow paths, age
685 distributions, and the paradoxical origins of the inverse storage effect in an experimental catchment, *Water Resources
686 Research*, 56, e2019WR025140, 2020.
- 687 Yang, M., Lee, J., Jang, S., Annable, M. D., and Jawitz, J. W.: Nitrate attenuation potential in karst conduits and aquifer
688 matrix, *Journal of Hydrology*, 624, 129896, 2023.
- 689